High-resolution neutron scattering study of $Tb_2Mo_2O_7$: A geometrically frustrated spin glass

G. Ehlers*
Spallation Neutron Source, Oak Ridge National Laboratory, Building 8600, Oak Ridge, Tennessee 37831-6475, USA

J. E. Greedan
Department of Chemistry and Brockhouse Institute for Materials Research, McMaster University, Hamilton, Ontario, Canada L8S 4M1

J. R. Stewart
ISIS Facility, Rutherford Appleton Laboratory, Chilton, Didcot OX11 0QX, United Kingdom

K. C. Rule
Helmholtz Zentrum Berlin, Hahn-Meitner Platz 1, 14109 Berlin, Germany

P. Fouquet
Institut Laue-Langevin, 6 rue Jules Horowitz, BP 156, 38042 Grenoble Cedex 9, France

A. L. Cornelius
Department of Physics, University of Nevada, Las Vegas, Nevada 89154-4002, USA

C. Adriano and P. G. Pagliuso
Instituto de Física Gleb Wataghin, Universidade Estadual de Campinas UNICAMP, Campinas, 13083-970 São Paulo, Brazil

Y. Qiu
Department of Materials Science and Engineering, University of Maryland, College Park, Maryland 20742, USA
and NCNR, NIST, Gaithersburg, Maryland 20899-6102, USA

J. S. Gardner
Department of Physics, Indiana University, Bloomington, Indiana 47408, USA
and NCNR, NIST, Gaithersburg, Maryland 20899-6102, USA

(Received 31 March 2010; revised manuscript received 3 May 2010; published 2 June 2010)

The low-temperature magnetic properties of $Tb_2Mo_2O_7$ have been studied with bulk susceptibility measurements and with elastic and high-resolution inelastic neutron scattering. This system is a spin glass with a freezing temperature $T_g \sim 25$ K. A reverse Monte Carlo simulation of the neutron diffraction data shows weak ferromagnetic near-neighbor spatial correlations that do not extend beyond $\lesssim 10$ Å. Neutron measurements of the spin dynamics reveal a slowing down with decreasing temperature without an anomaly at the glass transition. A low-lying Q-independent mode is seen at $\hbar\omega_0 \sim 0.28$ meV. This dispersionless crystal electric field transition is measurable up to 60 K.

DOI: 10.1103/PhysRevB.81.224405 PACS number(s): 75.40.Gb, 75.40.Mg, 75.50.Lk

I. INTRODUCTION

$Tb_2Mo_2O_7$ was one of the first magnets in which the impact of *geometrical frustration* on the low-temperature magnetic properties of a system was realized.[1–7] Such frustration is the consequence of a geometric arrangement of the magnetic moments in the lattice in a way that prevents the system from minimizing the energy of all near-neighbor bonds at the same time.[8–11] As a result, many nearly degenerate ground-state configurations typically exist in frustrated magnets, making them particularly susceptible to fluctuations. It is often observed that, if the system settles into an ordered ground state, the phase transition occurs only at a temperature much lower than the Curie-Weiss temperature (which indicates the energy scale of the various relevant magnetic interactions). However, the ground state is typically not one with conventional long-range order, the systems rather tend to enter a spin-glass or spin-liquid phase (which is to say that they remain dynamic, even though strong spatial correlations between magnetic moments may be present). In cases where long-range order does develop, exotic ordering patterns are sometimes observed, for example, in $Gd_2Ti_2O_7$ (Refs. 12–14) or $Tb_2Sn_2O_7$,[15–18] where long-range ordered and paramagnetic spin components coexist in the ground state.

The published work on $Tb_2Mo_2O_7$ established that this system is a spin glass with a freezing transition of $T_g \sim 25$ K (as determined by bulk measurements). The transition affects the magnetic moments associated with both sublattices (Tb^{3+} as well as Mo^{4+}), as no residual dynamics specifically due to one magnetic species has been reported.[4,7] Bulk measurements showed several key signatures of a spin-glass transition, such as a shift from the origin of a magnetic hysteresis loop, a disappearance of the thermoremanent magnetization at the glass temperature, and a logarithmic decay of the remanent magnetization.[5] A frequency shift of the sus-

 ©2010 The American Physical Society

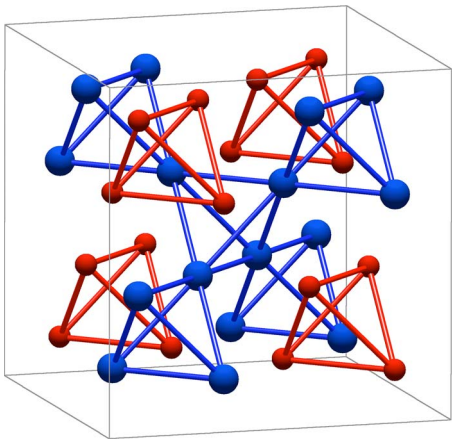

FIG. 1. (Color online) A unit cell of the pyrochlore lattice with 8 f.u. Both the rare earth and the transition metal (shown with large and small circles) form a lattice of corner sharing tetrahedra.

ceptibility peak, also typical for a spin glass, will be shown in Sec. III A of this paper.

$Tb_2Mo_2O_7$ adopts the cubic pyrochlore structure (space group $Fd\bar{3}m$), see Fig. 1. The formation of a spin-glass state is unexpected, as the samples show very good crystallinity and the most important form of structural disorder, a nonstoichiometric oxygen content, is estimated below 1% in good samples[4] (see Sec. II for the characterization of the sample used in this study). Traditionally, positional disorder is regarded a necessary ingredient for a spin glass to form. For isostructural $Y_2Mo_2O_7$, which is also a spin glass, this point has been extensively addressed.[19–23] A more detailed comparison between $Y_2Mo_2O_7$ and $Tb_2Mo_2O_7$ suggests, however, that the origin and details of the glassy state may be rather different between the two materials. First of all, in $Y_2Mo_2O_7$ there is only one magnetic lattice, and even though in $Tb_2Mo_2O_7$ the Mo-Tb exchange is expected to be weaker than the Mo-Mo exchange, it must have an impact through the large Tb moment and the associated internal magnetic field. Secondly, while T_g is similar for the two, ~22 K ($Y_2Mo_2O_7$) and ~25 K ($Tb_2Mo_2O_7$), the Weiss temperatures are very different: For $Y_2Mo_2O_7$ a large negative value $\theta_{CW} \sim -200$ K has been reported,[20] in contrast to the positive θ_{CW} for $Tb_2Mo_2O_7$ (see below in Sec. III A).

Neutron scattering experiments have been published previously on powder- and single-crystal samples of $Tb_2Mo_2O_7$.[2,4,7] Diffraction experiments revealed that the first, third and fourth near-neighbor interactions are all ferromagnetic (FM) while the second near-neighbor interaction (involving only Tb-Mo coupling) is antiferromagnetic (AFM). The Tb-Tb correlation length was estimated at $\sim 5 \pm 1$ Å,[4] independent of temperature below the glass transition. The crystal experiment revealed that the short-ranged spin arrangement actually resembles the spin ice structure but the Tb moments are slightly tilted off the local $\langle 111 \rangle$ direction.[7] In this study, the authors estimate that the static moment associated with the diffuse peaks at $T=1.6$ K is about $\sim 4\mu_B$, significantly less than what is expected for a Tb^{3+} ionic moment. The same study saw a strong diffuse background signal which the authors attributed to uncorrelated Tb moments.

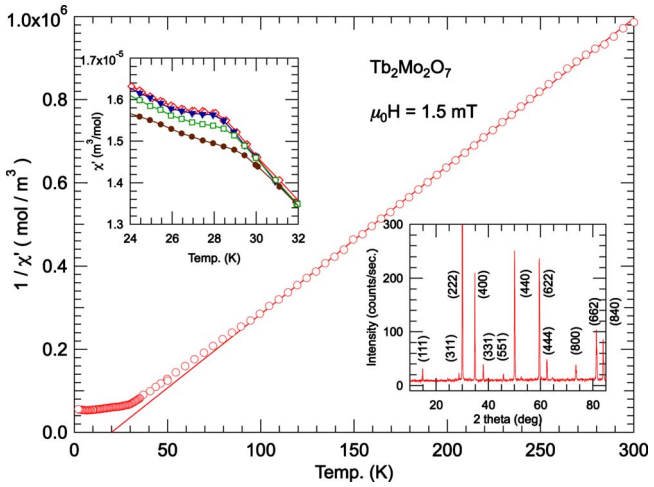

FIG. 2. (Color online) Sample characterization by susceptibility (main figure and top left insert) and x-ray diffraction (bottom right inset). The main figure shows the inverse susceptibility and the Curie-Weiss fit with the axis intercept. The top left insert shows the real part around the freezing temperature at different frequencies [(●) 50 Hz, (□) 100 Hz, (▼) 10^3 Hz, and (◇) 10^4 Hz].

It is important to realize that the early powder-diffraction experiment[2] missed the first correlation peak, as it occurs at unusually low wave vector Q, outside the accessible range of that experiment. Thus, as new data have become available, and the results of the above-mentioned studies are not in full agreement, we are motivated to revisit some of the previous analyses. We perform a reverse Monte Carlo (rmc) simulation of neutron diffraction data to study the ferromagnetic near-neighbor spatial Tb-Tb and Tb-Mo correlations and to derive a correlation length. We then present high-resolution quasielastic neutron scattering data that allow for a precise determination of the time scale of the spin fluctuations around the freezing transition.

II. EXPERIMENTAL

Polycrystalline samples were prepared by firing appropriate amounts of MoO_2 and Tb_4O_7 in a tube furnace at 1400 °C for 48 hours with a steady flow of a buffer gas made up of a 1:1 ratio of CO and CO_2. A more detailed account of the preparation process can be found in the literature.[1] It is important to stabilize the Mo^{4+} state in this process which appears to be successful when the cubic lattice constant is found to be 10.309(1) Å at room temperature (the correlation between oxygen stoichiometry and lattice constant has been discussed in Ref. 10) and the field-cooled and zero-field-cooled dc susceptibilities bifurcate at 25 K. It should be noted that, if the oxygen stoichiometry is off, creating defects and/or a different molybdenum valency, the lattice will expand and reveal the stoichiometry in the cubic lattice parameter. The room-temperature lattice constant, of our sample, determined by x-ray diffraction (see Fig. 2) was 10.312(5) Å indicating nearly ideal oxygen stoichiometry.

Neutron time-of-flight (TOF) spectra were taken at the disk chopper spectrometer (DCS) at the NCNR at NIST in

Gaithersburg.[24] An incident neutron wavelength of 5 Å was chosen, resulting in an elastic energy resolution of 94.3 μeV full width at half maximum (FWHM) and an accessible Q range of the scattering up to 2.4 Å^{-1}. A vanadium standard was used to measure the resolution and to correct the data for detector efficiency in a standard manner.

In the past it was shown that it is beneficial to combine neutron TOF with neutron spin-echo (NSE) data for the analysis of complex dynamics in a system. The strength of the NSE technique lies in the intrinsic separation of magnetic and nuclear scattering, and its sensitivity to fluctuations over a broad range of time scales.[25] NSE measurements were performed at the IN11C spectrometer at ILL, Grenoble, with an incident neutron wavelength of 5.5 Å ($\Delta\lambda/\lambda=15\%$).[26] Two settings of the multidetector array covered the Q range up to 1.3 Å^{-1}. The time range over which correlations could be studied extended from 4×10^{-12} s to 1×10^{-9} s. Additional NSE data were taken at NG5 at the NCNR at NIST at $Q=0.85$ Å^{-1} in a time range that extended to 1×10^{-8} s.

III. RESULTS

A. Susceptibility and specific heat

Figure 2 shows the temperature-dependent magnetic susceptibility obtained at $\mu_0 H=1.5$ mT. From this measurement, the bulk of the spin system freezes at $T_g\sim25$ K and has a frequency dependence of T_g of $\sim1.5\%$ per decade of the driving frequency f, a value that compares well with the canonical spin glass AuFe.[27] At high temperature a Curie-Weiss law is obeyed, $\chi^{-1}\propto(T-\theta_{\mathrm{CW}})$. A least squares fit to the data in the range 150 K$\leq T\leq$300 K gives a paramagnetic Curie-Weiss temperature $\theta_{\mathrm{CW}}=(20\pm1)$ K and a squared effective paramagnetic moment per formula unit of $p^2=169\pm1\mu_B^2$ (each formula unit contains two Mo^{4+} moments and two Tb^{3+} moments). Taking the $(S=1)$ Mo^{4+} moment from $Y_2Mo_2O_7$ as $\mu_{\mathrm{Mo}}\sim2.55\mu_B$,[20] the $(L=3,\ J=6)$ Tb^{3+} moment is computed to $\mu_{\mathrm{Tb}}\sim8.83\mu_B$. These results for the Curie-Weiss temperature and the magnetic moments are in reasonable agreement with earlier work. Published results for the Curie-Weiss temperature vary a little between samples: $\theta_{\mathrm{CW}}\sim+17$ K according to Ref. 1 and $\theta_{\mathrm{CW}}\sim+12$ K according to Ref. 7.

B. Elastic neutron scattering

In order to characterize the time-averaged spin correlations, the scattering function $S(Q,\omega)$ measured at DCS was integrated over the elastic resolution width, in the range ±0.1 meV. This is shown in the upper panel of Fig. 3. The dominant signature of the spin freezing is the development of a large correlation peak centered around $Q\sim0.25$ Å^{-1}. Two additional (much weaker) peaks, observed around $Q\sim1.1$ Å^{-1} and 1.7 Å^{-1}, respectively, were previously reported. Analysis of the temperature dependence of the first correlation peak suggests that spin-spin correlations develop between completely uncorrelated (paramagnetic) spins at 120 K.

The elastic scattering was analyzed using a rmc technique. For powder-averaged data, the scattering arising from

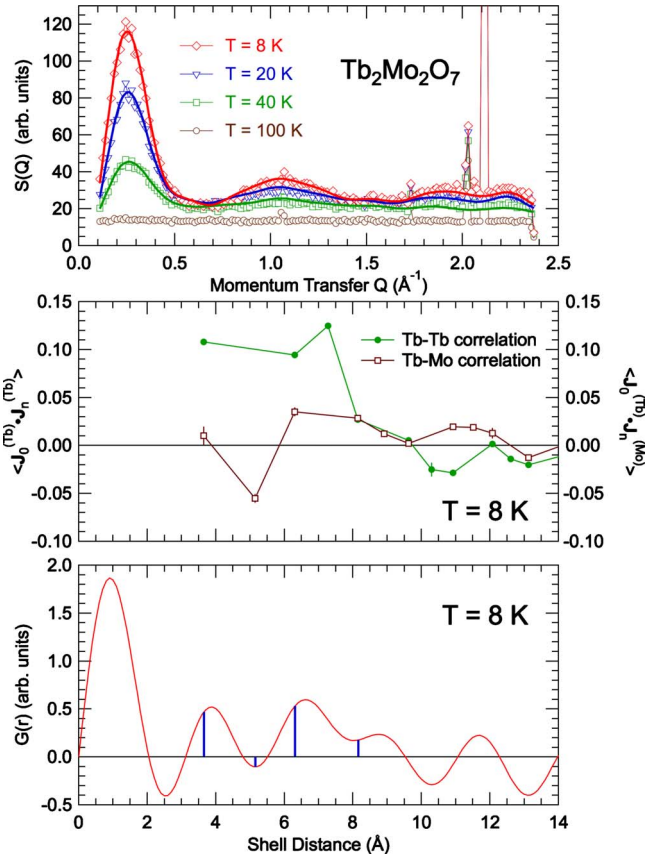

FIG. 3. (Color online) Top panel: the elastic scattering measured at DCS (integration range ±0.1 meV). The strong scattering at ~2.1 Å^{-1} is from the 222 Bragg peak. The lines represent the rmc fits. Middle panel: the normalized resulting shell correlations, $\langle \boldsymbol{J}_0^{(\mathrm{Tb})}\cdot\boldsymbol{J}_n^{(\mathrm{Tb})}\rangle$ and $\langle \boldsymbol{J}_0^{(\mathrm{Tb})}\cdot\boldsymbol{J}_n^{(\mathrm{Mo})}\rangle$, normalized such that "perfect" correlation corresponds to 1. Lower panel: the radial correlation function $G(r)$ (see text) at base temperature. The positions of the first four shell distances are marked.

the correlation of a given magnetic moment J_0 with near neighbors arranged in shells at distances R_n can be written as

$$S(Q)=\text{const.}\ f^2(Q)g_J^2J(J+1)\times\left\{1+\sum_n Z_n\frac{\langle \boldsymbol{J}_0\cdot\boldsymbol{J}_n\rangle}{J(J+1)}\frac{\sin(QR_n)}{QR_n}\right\},\qquad(1)$$

where $f(Q)$ is the magnetic form factor, J is the angular momentum quantum number, g_J is the Landé factor, and Z_n is the occupation in the nth shell.

If two types of magnetic moments are present in the lattice, such as Tb^{3+} and Mo^{4+} here, Eq. (1) can be expanded by two more sums to include all the $\langle \boldsymbol{J}_0^{(\mathrm{Tb})}\cdot\boldsymbol{J}_n^{(\mathrm{Tb})}\rangle$, $\langle \boldsymbol{J}_0^{(\mathrm{Tb})}\cdot\boldsymbol{J}_n^{(\mathrm{Mo})}\rangle$, and $\langle \boldsymbol{J}_0^{(\mathrm{Mo})}\cdot\boldsymbol{J}_n^{(\mathrm{Mo})}\rangle$ correlations (with the magnetic form factor properly adjusted). In the simulation, the moments were taken as $g_J\sqrt{J(J+1)}=8.83\mu_B$ for Tb^{3+} and $g_S\sqrt{S(S+1)}=2.55\mu_B$ for Mo^{4+} (see above). The Tb^{3+} form factor was taken from a standard reference.[28] The Mo^{4+} form factor was approximated as in Ref. 29.

The DCS data were obtained using unpolarized neutrons, and therefore the nuclear and magnetic scattering contribu-

tions are not separated. Since the total signal is used in the analysis, reliable results are only obtained if the magnetic scattering dominates. A comparison to a high-temperature data set (data at $T=100$ K, where the spin correlations have dissipated, are included in Fig. 3) provides an estimate of the elastic nuclear incoherent contribution to the scattering. In addition, from the NSE experiment (which uses polarization analysis) it is estimated that about 50% of the scattering at 100 K is nuclear. The nuclear scattering contribution is therefore small compared to the magnetic scattering at low temperature. This nuclear "background" was subtracted from the data before the simulation but is included in the display of the data as measured in Fig. 3.

The rmc simulation was performed on a cube of $6\times6\times6$ unit cells with magnetic moments situated at the 16*d* (Tb) and 16*c* (Mo) sites. The use of a larger ensemble, such as $8\times8\times8$ unit cells, did not significantly alter the results. No preferred moment direction in the lattice was assumed. Starting with an arbitrary spin configuration, a small number of spins was randomly chosen which were turned in one step of the simulation to a random new direction. A powder average of the scattering was then computed and fit with a single fit parameter (scale factor) to the data. This accounts for the fact that the measurement did not yield the scattering cross section in absolute units. The step was then accepted if the fit to the measured data was improved and repeated if not. Many individual rmc runs (with typically $\sim10^5$ steps) were performed until convergence and then linearly combined to produce the final best fit. The resulting fits are also shown in the upper panel in Fig. 3. The middle panel in the figure shows the resulting Tb-Tb and Tb-Mo spin correlations for the lowest temperature. These are normalized such that $\langle \boldsymbol{J}_0 \cdot \boldsymbol{J}_n \rangle = \pm 1$ would mean perfect FM/AFM correlation between two shells.

For a more direct comparison with the earlier result of such an analysis,[2] the real-space pairwise distribution function $G(r)$ was also computed from the data

$$G(r) = 2/\pi \int_{-\infty}^{+\infty} Q[S(Q)-1]\sin(Qr)dQ. \qquad (2)$$

This is shown in the lower panel of Fig. 3. The very limited Q range means that conclusions can only be drawn with care but the result agrees with the rmc analysis. Overall, the near-neighbor Tb-Tb correlations are ferromagnetic and short ranged, i. e. they do not reach beyond $\lesssim 10$ Å distance. The Tb-Mo correlations are antiferromagnetic in the second shell, in agreement with the earlier analysis,[2] and this seems to be what drives the system into the spin-glass state. Error bars resulting from a statistical analysis of the rmc runs (see above) are generally too small to be seen in the middle panel of Fig. 3 and therefore the result of an antiferromagnetic Tb-Mo correlation in the second shell appears to be robust. Since the Mo moment is much smaller, and thus scatters less, the Mo-Mo correlation cannot be determined reliably from the data. We do not see any signature of uncorrelated Tb moments, a conclusion that was put forward in Ref. 7, as the total diffuse intensity is accounted for in our analysis.

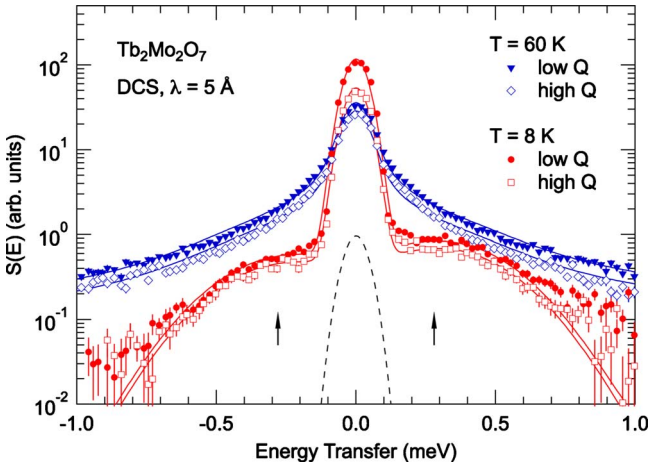

FIG. 4. (Color online) The background corrected quasielastic scattering measured at DCS with an energy resolution of 0.1 meV FWHM. This shows data integrated over both correlation peaks at 8 and at 60 K. Arrows mark the assumed position of the crystal-field excitation. The dashed line is the instrumental resolution. Fits are described in the text.

C. Quasielastic neutron scattering

For the analysis of the quasielastic scattering, the data were integrated over the Q ranges of the first two correlation peaks, from 0.1 Å^{-1} to 0.7 Å^{-1} ("low Q" peak) and from 0.7 Å^{-1} to 1.5 Å^{-1} ("high Q" peak), respectively. This is appropriate for the NSE data, which has coarse Q resolution, and allows for a simultaneous treatment of NSE and TOF data as described further below.

Figure 4 shows the quasielastic scattering, as obtained in the DCS measurement, at two temperatures. Here and in the following, error bars in the figures represent $\pm1\sigma$ from counting statistics. Three observations are immediately made: (i) at base temperature the scattering is clearly very different from the nearly Gaussian resolution. The most likely explanation is a low-lying crystal-field excitation giving rise to the additional scattering marked with arrows. This is discussed further below. (ii) At higher temperature a quasielastic process provides additional scattering intensity at finite energy transfer (outside the elastic resolution window) which is absent at base temperature in the frozen spin-glass state. (iii) The only Q dependence is in the elastic intensity, the spin dynamics manifest in the broadening of the spectra is independent of Q.

The measured intensity $S^{(\mathrm{DCS})}(E)$ was analyzed in terms of a numerical convolution of the scattering function $S(E)$ and the instrumental resolution $R(E)$, measured with vanadium

$$S^{(\mathrm{DCS})}(E) = \{S(E)n(E)\} \otimes R(E),$$

where $n(E)=(E/k_\mathrm{B}T)[1-\exp(-E/k_\mathrm{B}T)]^{-1}$ is the thermal population factor and

$$S(E) = (I_{\mathrm{mag}} + I_{\mathrm{nuc}}) \cdot \delta(0) + I_{\mathrm{CF}}\{g(-\hbar\omega_0) + g(+\hbar\omega_0)\} + I_{\mathrm{QE}} \cdot \mathcal{F}\{\exp(-[t/\tau]^{\beta})\} \quad (3)$$

is a sum of three terms: (1) elastic scattering within the resolution with magnetic intensity I_{mag} and nuclear intensity I_{nuc}, (2) a low-energy ($\hbar\omega_0 \sim 0.28$ meV) crystal-field excitation with intensity I_{CF}, approximated as a pair of Gaussians $g(\pm\hbar\omega_0)$, and (3) a quasielastic process modeled as a stretched exponential spin relaxation with an intensity I_{QE}, $\mathcal{F}$ denotes the Fourier transform.

With TOF one measures the sum $I_{\mathrm{mag}}+I_{\mathrm{nuc}}$ whereas in an NSE experiment one separates the two contributions, measuring only I_{mag}. Neglecting $n(E)$, which is appropriate for the ~ 1 μeV energy resolution of the NSE measurement at ~ 2 K and higher, the corresponding intermediate scattering function $I(t)$ measured with NSE reads

$$I(t)/I(0) = I_{\mathrm{mag}}/I(0) + I_{\mathrm{CF}}/I(0) \cdot \mathcal{F}^{-1}\{g(\pm\hbar\omega_0)\} + I_{\mathrm{QE}}/I(0)\exp(-[t/\tau]^{\beta}), \quad (4)$$

where the sum $I(0)=I_{\mathrm{mag}}+I_{\mathrm{CF}}+I_{\mathrm{QE}}$ provides the traditional normalization of the NSE signal $I(t)$ to 1.

The ultimate goal of the analysis of the quasielastic scattering is to determine the temperature dependence of the spin-relaxation time (or its distribution). To achieve this, two types of fits to the data were performed. (i) The TOF spectra at all measured temperatures between 8 and 120 K were fit simultaneously to the model of Eq. (3), allowing only the intensities and the parameter τ to vary with temperature. In the second step, the τ parameter was then constrained for each pair (low Q vs high Q peak) of data sets to be the same, to be consistent with the initial observation of a Q-independent dynamics. (ii) At temperatures where NSE and TOF data were both available (20 and 40 K, at higher temperature the scattering is too inelastic for NSE), TOF and NSE data sets were fit simultaneously, minimizing the sum of the individual χ^2 values. The results of these latter fits are shown in Fig. 5.

As discussed earlier, a dispersionless mode can be seen at an energy $\hbar\omega_0 \sim 0.28$ meV (3.2 K) at the base temperature of the inelastic neutron scattering experiment (8 K). The intensity of this excitation is small compared to the other scattering contributions, $I_{\mathrm{CF}}/I(0) \sim 3\%$ and its inverse Fourier transform used in Eq. (4) decays to zero at 1×10^{-11} s, near the low end of the NSE time range.[33] The excitation is too small to be clearly resolved within the resolution of the TOF measurement but is phenomenologically described by a Gaussian $g(\hbar\omega_0)$ with FWHM ~ 0.51 meV whose parameters were determined at base temperature and then fixed for all fits. The intensity of this mode decreases monotonically with increasing temperature, tracking the intensity of the first correlation peak and merges into the quasielastic scattering above 60 K. The isostructural systems $Tb_2Ti_2O_7$ and $Tb_2Sn_2O_7$ possess a low-lying crystal-field excitation at ~ 1.5 meV and ~ 1.2 meV, respectively, which corresponds to the transition from the ground state to the first excited doublet.[18,34,35] In $Tb_2Mo_2O_7$ such an excitation has previously been unsuccessfully searched for between 0.5 and 4 meV.[7] Our results confirm these earlier findings. The disparity between $Tb_2Mo_2O_7$ on one hand and the stannate and titanate on the other hand is surprising since the local environment of the Tb^{3+} ion is very similar in all three systems. In both the stannate and titanate, when the electronic spin system orders, the ground-state doublet splits, resulting in a low-lying dispersionless mode at a few hundred μeV.[18,36,37] The temperature dependence of the 0.28 meV excitation suggests that it is also the result of the Tb ground-state doublet being split in a molecular field generated by the spin-spin correlations that develop at low temperature.

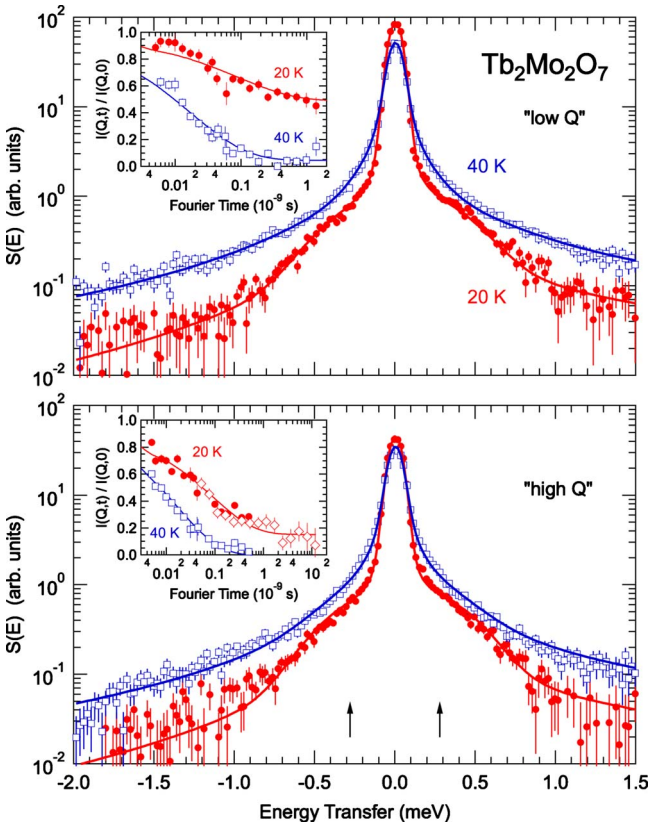

FIG. 5. (Color online) The quasielastic scattering from both TOF and NSE analyzed simultaneously at 20 and 40 K. The main panels show the background corrected TOF spectra at the lower Q (in the upper panel) and the higher Q (lower panel), respectively. The arrows show the position of the excitation associated with a transition between CEF levels. The insets show the NSE spectra measured at the same temperature. In the lower inset an NSE data set from NIST ($\diamond$) is included that extends the Fourier time range to 10 ns.

The spin relaxation is phenomenologically described by a stretched exponential function with a temperature-independent exponent, $\beta \sim 0.5$. This provides an adequate description for our data. This model function is commonly used for spin glasses and structural glasses, and is a special case of a more general functional form recently discussed.[38] In our case, a more detailed analysis of the line shape cannot be done mostly because the NSE data lacks dynamic range.

The temperature dependence of the spin-relaxation time resulting from the fits described above is displayed in Fig. 6. Fitting with and without NSE data gives consistent results within the accuracy that can normally be achieved in such an

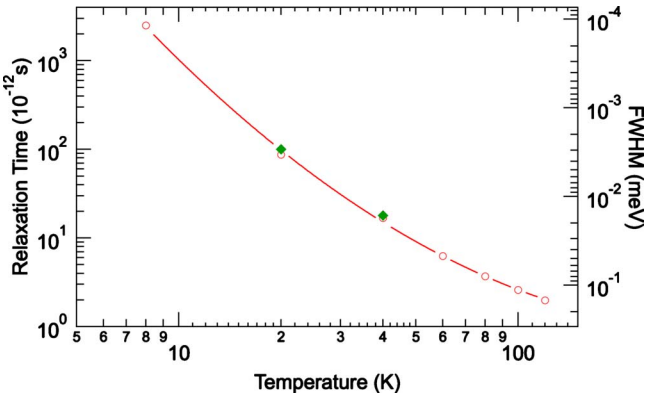

FIG. 6. (Color online) The temperature dependence of the spin-relaxation time. Open symbols: fits to the DCS data. Full symbols: combined fits to DCS and NSE data as described in the text. The line is a guide to the eye. The right axis shows the FWHM (resolution deconvoluted) on the energy axis, which for a stretched exponential relaxation function with an exponent $\beta=0.5$ follows the empirical relation FWHM(meV)$=0.2943/\tau$(ps).

analysis. As the temperature is lowered, the spin ensemble becomes increasingly slow, which is expected, but without noticeable anomaly at the glass temperature $T_g \sim 25$ K determined by bulk methods.

IV. DISCUSSION

We start by putting $Tb_2Mo_2O_7$ into context with the entire $R_2Mo_2O_7$ series where R is a rare earth. Table I below lists those ternary systems for which the cubic pyrochlore structure has been reported. Ionic radii have been taken from Ref. 39. Data for bond angles are from Ref. 40 and our own unpublished data.

Systems with large r_R of the rare earth (including $Eu_2Mo_2O_7$) are metallic and ferromagnetic at low temperature with a reentrant spin-glass phase and anomalous transport properties.[30–32] $Tb_2Mo_2O_7$ is the first insulating and nonferromagnetic member of the series. All subsequent series members are also nonmetallic and spin glassy. Of this latter group, $Y_2Mo_2O_7$ has been studied in most detail. The Curie temperatures of the metallic ferromagnets decrease with decreasing r_R as 100 K (Nd), 93 K (Sm), and 82 K (Gd). In contrast, the spin-glass-transition temperatures are flat across the second part of the series. For example, $T_g \sim 21$ K for $Ho_2Mo_2O_7$ and $T_g \sim 17$ K for $Yb_2Mo_2O_7$.[41,42] Detailed studies of the spin-glass states by scattering methods have only been published for the Tb and Y systems.

TABLE I. Structure data for members of the $R_2Mo_2O_7$ series for which the cubic pyrochlore structure has been reported. The bond angle was computed from the oxygen site parameter x, where available.

R^{3+}	r_R (Å)	x	Mo-O-Mo angle	Ground state
Nd	1.109	0.3297(7)	131.5	Metallic
Sm	1.079	0.3300(5)	131.3	Metallic
Eu	1.066			Metallic
Gd	1.053	0.3315(8)	130.5	Metallic
Tb	1.040	0.3363(2)	128.0	Insulating
Dy	1.027	0.3331(6)	129.7	Insulating
Y	1.019	0.3382(1)	126.9	Insulating
Ho	1.015	0.3385(2)	126.8	Insulating
Er	1.004	0.3392(2)	126.4	Insulating
Tm	0.994			Insulating
Yb	0.985			Insulating
Lu	0.977			Insulating

It may be argued that the origin and details of the glassy state should be different between these two materials. $Tb_2Mo_2O_7$ is close to the phase boundary to ferromagnetic systems in the $R_2Mo_2O_7$ family of compounds. This is reflected in the positive Curie-Weiss temperature, $\theta_{CW} \sim +20$ K (see above), which is very different from $\theta_{CW} \sim -200$ K for $Y_2Mo_2O_7$. Our analysis of the magnetic shell correlations from the static diffuse neutron scattering data shows that the near-neighbor Tb-Tb correlations are weakly ferromagnetic to the fourth shell and the correlation length is ≤ 10 Å in good agreement with the earlier result.[4] We do confirm that the Tb-Mo correlation in the second shell is strongly antiferromagnetic as previously reported.[2] The competition of near-neighbor AFM/FM correlations thus may be what is driving $Tb_2Mo_2O_7$ into the spin-glass state. On the other hand, in $Y_2Mo_2O_7$ there is only one magnetic lattice and here the spin-glass state is likely stabilized by bond length disorder.[20–23] The presence of subtle disorder in $Tb_2Mo_2O_7$ cannot be ruled out at this stage as relevant studies do not exist.

New quasielastic neutron scattering data reveal spin dynamics independent of momentum transfer Q. There is no evidence for different time scales of the fluctuations in the Tb and Mo sublattices although the Mo sublattice is nearly impossible to detect with the Tb moment dominating the magnetic signal. The spin-fluctuation rate at the glass temperature T_g is estimated at $1/2\tau(25\ \text{K}) \sim 1 \times 10^{10}$ Hz. This value is very close to what was found with NSE in $Y_2Mo_2O_7$ (0.7×10^{10} Hz at 25 K) with $T_g \sim 22$ K.[43] It is also remarkably close to the result of μSR work on $Tb_2Mo_2O_7$ which found 0.01 THz at 25 K.[6] Cooling the system below the glass transition leads to a gradual freezing of the moments but at $T=8$ K the time scale of the fluctuations is still in the measurement window of the neutron scattering technique. The muon work followed persistent spin relaxation down to a temperature of ≤ 0.1 K but this cannot be confirmed with neutrons at the present time.

We have observed the first low-lying magnetic excitation in this system. Below 60 K a crystal electric field (CEF) transition from the ground state to the first excited state can be seen at an energy $\hbar\omega_0 \sim 0.28$ meV. This energy is similar to that seen in isostructural $Tb_2Ti_2O_7$ and $Tb_2Sn_2O_7$ materials when they are magnetically ordered. Although more studies are required to determine the full crystal-field Hamiltonian, it is believed that the doublet ground state splits as an internal field develops due to the slow, if not static, short-range spin-spin correlations that develop.

V. CONCLUSION

Polycrystalline $Tb_2Mo_2O_7$ with a cubic lattice parameter of 10.312 Å has been studied by neutron scattering and ac susceptibility. The glassy, bulk freezing has been investigated. Spin correlations develop below 60 K and never extend beyond 10 Å. The first and third neighbor correlations are ferromagnetic but the second shell (involving only Tb-Mo coupling) is antiferromagnetic. Neutron spin echo and time-of-flight techniques revealed a multitude of relaxation processes with mean spin-relaxation time around 10^{-9} s at 10 K. Although a study of the local crystal structure is warranted, our results for the spin-spin correlations, by reverse Monte Carlo and radial correlation function, suggest that the combination of ferromagnetic near-neighbor and antiferromagnetic next-nearest-neighbor correlations cause the glassiness in the system.

ACKNOWLEDGMENTS

This Research at Oak Ridge National Laboratory's Spallation Neutron Source was sponsored by the Scientific User Facilities Division, Office of Basic Energy Sciences, U. S. Department of Energy. The NCNR is in part funded by the National Science Foundation under Agreement No. DMR-0454672. We thank A. D. Lozano-Gorrin and S. Derahkshan for sample preparation. J.E.G. thanks NSERC. The authors are grateful for the local support staff at the ILL and at NIST.

*Corresponding author; ehlersg@ornl.gov

[1] M. Sato, X. Yan, and J. E. Greedan, Z. Anorg. Allg. Chem. **540-541**, 177 (1986).
[2] J. E. Greedan, J. N. Reimers, S. L. Penny, and C. V. Stager, J. Appl. Phys. **67**, 5967 (1990).
[3] J. E. Greedan, J. N. Reimers, C. V. Stager, and S. L. Penny, Phys. Rev. B **43**, 5682 (1991).
[4] B. D. Gaulin, J. N. Reimers, T. E. Mason, J. E. Greedan, and Z. Tun, Phys. Rev. Lett. **69**, 3244 (1992).
[5] N. Ali, P. Hill, X. Zhang, and F. Willis, J. Alloys Compd. **181**, 281 (1992).
[6] S. R. Dunsiger, R. F. Kiefl, K. H. Chow, B. D. Gaulin, M. J. P. Gingras, J. E. Greedan, A. Keren, K. Kojima, G. M. Luke, W. A. MacFarlane, N. P. Raju, J. E. Sonier, Y. J. Uemura, and W. D. Wu, Phys. Rev. B **54**, 9019 (1996).
[7] D. K. Singh, J. S. Helton, S. Chu, T. H. Han, C. J. Bonnoit, S. Chang, H. J. Kang, J. W. Lynn, and Y. S. Lee, Phys. Rev. B **78**, 220405(R) (2008).
[8] A. P. Ramirez, in *Handbook of Magnetic Materials*, edited by K. H. J. Buschow (Elsevier, Amsterdam, 2001), Chap. 4.
[9] *Frustrated Spin Systems*, edited by H. T. Diep (World Scientific, Singapore, 2004).
[10] J. S. Gardner, M. J. P. Gingras, and J. E. Greedan, Rev. Mod. Phys. **82**, 53 (2010).
[11] L. Balents, Nature (London) **464**, 199 (2010).
[12] J. D. M. Champion, A. S. Wills, T. Fennell, S. T. Bramwell, J. S. Gardner, and M. A. Green, Phys. Rev. B **64**, 140407(R) (2001).
[13] A. P. Ramirez, B. S. Shastry, A. Hayashi, J. J. Krajewski, D. A. Huse, and R. J. Cava, Phys. Rev. Lett. **89**, 067202 (2002).
[14] J. R. Stewart, G. Ehlers, A. S. Wills, S. T. Bramwell, and J. S. Gardner, J. Phys.: Condens. Matter **16**, L321 (2004).
[15] I. Mirebeau, A. Apetrei, J. Rodríguez-Carvajal, P. Bonville, A. Forget, D. Colson, V. Glazkov, J. P. Sanchez, O. Isnard, and E. Suard, Phys. Rev. Lett. **94**, 246402 (2005).
[16] P. Dalmas de Réotier, A. Yaouanc, L. Keller, A. Cervellino, B. Roessli, C. Baines, A. Forget, C. Vaju, P. C. M. Gubbens, A. Amato, and P. J. C. King, Phys. Rev. Lett. **96**, 127202 (2006).
[17] F. Bert, P. Mendels, A. Olariu, N. Blanchard, G. Collin, A. Amato, C. Baines, and A. D. Hillier, Phys. Rev. Lett. **97**, 117203 (2006).
[18] K. C. Rule, G. Ehlers, J. R. Stewart, A. L. Cornelius, P. P. Deen, Y. Qiu, C. R. Wiebe, J. A. Janik, H. D. Zhou, D. Antonio, B. W. Woytko, J. P. Ruff, H. A. Dabkowska, B. D. Gaulin, and J. S. Gardner, Phys. Rev. B **76**, 212405 (2007).
[19] A. Keren and J. S. Gardner, Phys. Rev. Lett. **87**, 177201 (2001).
[20] J. S. Gardner, B. D. Gaulin, S.-H. Lee, C. Broholm, N. P. Raju, and J. E. Greedan, Phys. Rev. Lett. **83**, 211 (1999).
[21] C. H. Booth, J. S. Gardner, G. H. Kwei, R. H. Heffner, F. Bridges, and M. A. Subramanian, Phys. Rev. B **62**, R755 (2000).
[22] E. Sagi, O. Ofer, A. Keren, and J. S. Gardner, Phys. Rev. Lett. **94**, 237202 (2005).
[23] J. E. Greedan, D. Gout, A. D. Lozano-Gorrin, S. Derahkshan, Th. Proffen, H.-J. Kim, E. Božin, and S. J. L. Billinge, Phys. Rev. B **79**, 014427 (2009).
[24] J. R. D. Copley and J. C. Cook, Chem. Phys. **292**, 477 (2003).
[25] G. Ehlers, J. Phys.: Condens. Matter **18**, R231 (2006).
[26] B. Farago, Physica B **397**, 91 (2007).
[27] J. A. Mydosh, *Spin Glasses—An Experimental Introduction* (Taylor & Francis, London, 1993), p. 64.
[28] P. J. Brown, *Magnetic Form Factors*, International Tables for Crystallography Vol. C, edited by A. J. C. Wilson (Kluwer Academic, Dordrecht, The Netherlands, 1996), Chap. 4.4.5, p. 391–399.
[29] M. K. Wilkinson, E. O. Wollan, H. R. Child, and J. W. Cable, Phys. Rev. **121**, 74 (1961).
[30] N. Hanasaki, M. Kinuhara, I. Kézsmárki, S. Iguchi, S. Miyasaka, N. Takeshita, C. Terakura, H. Takagi, and Y. Tokura, Phys. Rev. Lett. **96**, 116403 (2006).
[31] N. Hanasaki, K. Watanabe, T. Ohtsuka, I. Kézsmárki, S. Iguchi, S. Miyasaka, and Y. Tokura, Phys. Rev. Lett. **99**, 086401 (2007).
[32] S. Iguchi, N. Hanasaki, M. Kinuhara, N. Takeshita, C. Terakura, Y. Taguchi, H. Takagi, and Y. Tokura, Phys. Rev. Lett. **102**, 136407 (2009).
[33] The inverse Fourier transform has to take into account the coarse wavelength resolution of the NSE experiment. For this reason, any oscillations of the signal are very rapidly quenched.
[34] J. S. Gardner, S. R. Dunsiger, B. D. Gaulin, M. J. P. Gingas, J. E. Greedan, R. F. Kiefl, M. D. Lumsden, W. A. MacFarlane, N. P. Raju, J. E. Sonier, I. Swainson, and Z. Tun, Phys. Rev. Lett. **82**, 1012 (1999).
[35] I. Mirebeau, P. Bonville, and M. Hennion, Phys. Rev. B **76**,

184436 (2007).
[36] K. C. Rule, J. P. C. Ruff, B. D. Gaulin, S. R. Dunsiger, J. S. Gardner, J. P. Clancy, M. J. Lewis, H. A. Dabkowska, I. Mirebeau, P. Manuel, Y. Qiu, and J. R. D. Copley, Phys. Rev. Lett. **96**, 177201 (2006).
[37] K. C. Rule, G. Ehlers, J. S. Gardner, Y. Qiu, E. Moskvin, K. Kiefer, and S. Gerischer, J. Phys.: Condens. Matter **21**, 486005 (2009).
[38] R. M. Pickup, R. Cywinski, C. Pappas, B. Farago, and P. Fouquet, Phys. Rev. Lett. **102**, 097202 (2009).
[39] R. D. Shannon, Acta Crystallogr., Sect. A: Cryst. Phys., Diffr., Theor. Gen. Crystallogr. **32**, 751 (1976).
[40] Y. Moritomo, S. Xu, A. Machida, T. Katsufuji, E. Nishibori, M. Takata, M. Sakata, and S.-W. Cheong, Phys. Rev. B **63**, 144425 (2001).
[41] K. Miyoshi, Y. Nishimura, K. Honda, K. Fujiwara, and J. Takeuchi, Physica B **284-288**, 1463 (2000).
[42] J. A. Hodges, P. Bonville, A. Forget, J. P. Sanchez, P. Vulliet, M. Rams, and K. Królas, Eur. Phys. J. B **33**, 173 (2003).
[43] J. S. Gardner, G. Ehlers, R. H. Heffner, and F. Mezei, J. Magn. Magn. Mater. **226-230**, 460 (2001).